

## Transient aerodynamic forces of a vehicle passing through a bridge tower's wake region in crosswind environment

Lin Ma<sup>1</sup>, Dajun Zhou<sup>1</sup>, Wanshui Han<sup>\*2</sup>, Jun Wu<sup>2</sup> and Jianxin Liu<sup>2</sup>

<sup>1</sup>Department of Civil Engineering, University of Hohai, No.1 Xikang Road, Nanjing, Jiangsu 210098, China

<sup>2</sup>Department of Bridge Engineering, University of Chang'an, Middle of S.2nd Ring Road, Xi'an, Shanxi 710064, China

(Received March 30, 2015, Revised November 27, 2015, Accepted December 17, 2015)

**Abstract.** Super long-span bridges provide people with great convenience, but they also bring traffic safety problems caused by strong wind owing to their high decks. In this paper, the large eddy simulation together with dynamic mesh technology in computational fluid dynamics (CFD) is used to explore the mechanism of a moving vehicle's transient aerodynamic force in crosswind, the regularity and mechanism of the vehicle's aerodynamic forces when it passes through a bridge tower's wake zone in crosswind. By comparing the calculated results and those from wind tunnel tests, the reliability of the methods used in the paper is verified on a moving vehicle's aerodynamic forces in a bridge tower's wake region. A vehicle's aerodynamic force coefficient decreases sharply when it enters into the wake region, and reaches its minimum on the leeward of the bridge tower where exists a backflow region. When a vehicle moves on the outermost lane on the windward direction and just passes through the backflow region, it will suffer from negative lateral aerodynamic force and yaw moment in the bridge tower's wake zone. And the vehicle's passing ruins the original vortex structure there, resulting in that the lateral wind on the right side of the bridge tower does not change its direction but directly impact on the vehicle's windward. So when the vehicle leaves from the backflow region, it will suffer stronger aerodynamic than that borne by the vehicle when it just enters into the region. Other cases of vehicle moving on different lane and different directions were also discussed thoroughly. The results show that the vehicle's pneumatic safety performance is evidently better than that of a vehicle on the outermost lane on the windward.

**Keywords:** CFD (computational fluid dynamics); bluff body; cable-stayed bridge; large eddy simulation (LES); aerodynamic problem

### 1. Introduction

The bridge engineering has entered a new era of constructing sea-crossing projects around the world in the 21st century. In order to bypass building foundations in deep sea, long-span bridges become a preferred choice in sea-crossing engineering projects. However, there are several problems which need further study to guarantee the serviceability and safety of the long-span bridge. One primary problem is on the driving safety and comfort of the vehicles under the crosswind. Especially, a vehicle that goes through a bridge's tower in a windy environment, will

---

\*Corresponding author, Professor, E-mail: [hws-freedom@163.com](mailto:hws-freedom@163.com)

experience sharp changes of transient aerodynamic forces and even encounter the action of the negative lateral force and yawing moment in the tower's wake region. Additionally, when a vehicle overtakes or meets another vehicle on a bridge deck in crosswind, it will encounter a quite strong lateral aerodynamic interference and its aerodynamic forces will also experience sharp changes in a short period of time. All these factors induce disadvantageous influences on the vehicle's driving safety. Thus, it is important to study the transient aerodynamic mechanism and influencing factors of a moving vehicle in crosswind and explore the regularity of moving vehicles' aerodynamic interference, which will promote the traffic safety of vehicles on the sea-crossing bridges in a strong wind environment.

In order to investigate the problems of traffic safety on a bridge and etc., Xu and Guo (2003) studied the safety problem of a vehicle moving on a bridge deck in a windy environment by establishing a complicated wind-vehicle-bridge coupling vibration analysis system. Chen and Cai (2004) also studied the problem using vehicle-bridge coupling analysis, which further considered the influence of driver behavior. Rocchi *et al.* (2012) studied a vehicle's driving safety performance when it crosses a bridge tower's wake zone by using the measured aerodynamic force in wind tunnel testing. Han and Ma (2010a, 2011, 2015) studied the lateral coupling relation between the vehicle-bridge systems under crosswind, the wind-vehicle-bridge system considering driver behavior, and the nonlinear performance simulation of super-long-span cable-stayed under traffic and wind. Cai *et al.* (2013, 2015) provided a comprehensive review of the overall performance of the bridge and traffic system under strong wind, including bridge structures and vehicles, and the associated mitigation efforts.

During the past decade, researchers have paid more attention to the aerodynamic forces on vehicles on a bridge deck in crosswind and the aerodynamic interference between vehicles and a bridge. Bettle *et al.* (2003) examined the effect of truck speed on the aerodynamic forces acting on a standard sized, North American transport truck traveling on a bridge in crosswind by using computational fluid dynamics (CFD). Charuvisit *et al.* (2004a) obtained the transient aerodynamic forces of vehicles going through bridge towers' wake zone by using moving vehicle models in a wind tunnel. Charuvisit *et al.* (2004b) studied the influence of wind barrier on the transient aerodynamic forces of a moving vehicle model using the wind tunnel tests. Li *et al.* (2009) presented a new experimental setup considering the movement of vehicles to measure the aerodynamic forces of a moving vehicle-bridge system under the cross wind. Li *et al.* (2010) used CFD to simulate the wind field above the bridge deck nearby the towers of a long-span suspension bridge. Based on the wind field distribution from the CFD and the measured aerodynamic coefficients from a wind tunnel test, they adopted a self-developed analysis software BANSYS to conduct a contrast analysis for the dynamic responses of vehicles running through a bridge tower along different rail positions.

Zhu *et al.* (2012) studied aerodynamic force coefficients of four types of road vehicles on a typical bridge deck by using wind tunnel tests. The aerodynamic coefficients of the same road vehicles on the ground are also provided to explore the effects of the bridge deck on aerodynamic coefficients. The effects of vehicle position in different road lanes of the bridge deck are investigated. Wang *et al.* (2013) reported the use of computational fluid dynamics (CFD) to simulate the aerodynamic forces on coupled vehicle-bridge deck systems under crosswinds. The aerodynamic coefficients of a stationary vehicle-deck system were simulated and then compared with wind tunnel results. A relative velocity method was then used to obtain the aerodynamic forces of a moving vehicle-deck system. The moving effects on the aerodynamic forces on the vehicle-deck system were evaluated.

Han *et al.* (2013) also developed an experimental setup to measure the aerodynamic characteristics of vehicles and the bridge in a wind tunnel considering the aerodynamic interference. Based on the experimental results, the influence of the wind turbulence, the wind speed and the vehicle position on the aerodynamic coefficients of vehicles, and the influence of vehicles on the static coefficients of the bridge were investigated. Han *et al.* (2014) further fitted the aerodynamic force coefficients of the vehicle considering the aerodynamic interference between vehicles and the bridge, and provided a more effective and accurate approach to estimate the performance of vehicles on a bridge deck. In the literature (Han *et al.* 2015) the influence of vehicles on the flutter derivatives and the critical flutter wind velocity of bridges is explored.

In addition, Snæbjörnsson *et al.* (2007) researched the probability evaluation of road vehicle safety in windy environments. Han and Ma (2010b) studied the probability of wind-induced vehicle accidents on a bridge deck based on joint distribution of wind speed and wind direction. Ma *et al.* (2013) also studied the overturning probability assessment problem of a van moving on a bridge deck in crosswind environments, which considered the stochastic influence of turbulent wind and bridge deck' roughness by using dynamic reliability theory.

Lots of progresses have been made on the vehicle's aerodynamic forces in crosswind based on wind tunnel experiments and numerical simulations. However, existing researches paid less attention to the mechanism of transient aerodynamic forces and the regularity of dynamic aerodynamic interferences. Given that the computational fluid dynamics (CFD) can conveniently provide such information as the distribution of flow velocity and wind pressure, this paper uses CFD to study the mechanism of a moving vehicle's transient aerodynamic force in crosswind, the regularity and mechanism of the aerodynamic force encountered by a moving vehicle through a bridge tower's wake region. In the following parts, the numerical analysis method is introduced firstly. Next, the numerical model is validated by the wind tunnel tests. Then, the mechanism of the moving vehicle's transient aerodynamic forces in crosswind is studied and compared with that of the stationary vehicle. Finally, the regularity and mechanism is investigated of the aerodynamic force of the moving vehicle in the bridge tower's wake region.

## **2. Theoretical basis of CFD model**

Computational Fluid Dynamics (CFD) is an important branch of Fluid mechanics. It analyzes the physical phenomena such as fluid flow and heat transfer by numerical calculation and graphic display in computer, which has become a powerful tool to analyze the fluid problem. In the following, the CFD methods adopted in this study is introduced.

### *2.1 Turbulence model*

Turbulence is the most common flow patterns in nature and engineering field, and it is a complex three dimensional unsteady flow. Its various physical quantities, such as flow velocity, flow pressure, etc., present the characteristics of random. There are three methods to conduct the numerical simulation of turbulence: Direct Numerical Simulation (DNS), Reynolds-Averaged Navier-Stokers simulation (RANS) and Large Eddy Simulation (LES).

The DNS is the method of solving the 3D unsteady N-S equations directly, without using any approximate turbulence model. DNS method is generally used for the fundamental research about turbulence, such as discovering new structure, revealing the new mechanism and improving the

turbulence model, etc. But turbulent direct simulation has always been limited by the computer's speed and capacity. The non-direct numerical simulation does not directly solve all turbulent fluctuation, but tries to simplify the problem to some degree and do some approximate treatment, in which the widely-applied methods in engineering are large eddy simulation (LES) and Reynolds-averaged Navier-Stokes simulation (RANS). RANS decomposes turbulent motion as the time-averaged current and the instantaneous pulse current. In the time-averaged Navier-Stokes equations, there are six Reynolds stress items, which reflect the influence of instantaneous pulse on time averaged flow. The existence of the Reynolds stress terms makes Navier-Stokes equations not closed, and thus the turbulence model is needed to make them closed. The widely-used turbulence models include standard  $k$  - epsilon model and RNG  $k$  - epsilon model, etc. Large eddy simulation (LES) is a compromise method between DNS and RANS method. Its computation work is less than DNS, and generally greater than RANS. For the fluid problem with the flow separation, circulation and shedding vortex, LES is better than RANS method (Breuer *et al.* 2008). This paper adopts LES to investigate the unsteady aerodynamic force and interference encountered by a moving vehicle, which is a flow problem around blunt bodies. The principle of LES is introduced in the following part.

## 2.2 Large eddy simulation

Through the establishment of a mathematical filtering function, large eddy simulation (LES) filters out the vortices smaller than the filtering function's scale from the instantaneous equations of motion and arrived at the large eddy current equations of motion. The effects of small filtered-out vortices on large vortices' motion are taken into consideration through introducing additional stress in movement equations. By integrating transient Navier-stokes equation and continuity equation using the filter function, their time-averaged forms could be given as follows

$$\frac{\partial}{\partial t}(\rho \bar{u}_i) + \frac{\partial}{\partial x_j}(\rho \bar{u}_i \bar{u}_j) = \frac{\partial}{\partial x_j} \left( \mu \frac{\partial \bar{u}_i}{\partial x_j} \right) - \left( \frac{\partial \bar{p}}{\partial x_i} + \frac{\partial \tau_{ij}}{\partial x_j} \right) \quad (1)$$

$$\frac{\partial \rho}{\partial t} + \frac{\partial}{\partial x_i}(\rho \bar{u}_i) = 0 \quad (2)$$

where the bar over the physical quantity indicates the spatial filtering operation for LES;  $\rho$ ,  $t$  and  $\mu$  denote density, time and kinetic viscosity, respectively;  $u_i$  ( $i = 1, 2, 3$ ) represent the speed in  $x$ ,  $y$  and  $z$  direction. Four items in the momentum equations are transient item, convective item, diffusive item and the source item, successively;  $\tau_{ij}$  is similar to Reynolds stress in Reynolds averaged method, which embodies the effects of small-scale vortices on fluid motion and is called sub-grid scale stress (SGS). Its expression formula is as follows

$$\tau_{ij} = \overline{\rho u_i u_j} - \rho \bar{u}_i \bar{u}_j \quad (3)$$

The widely-used sub-grid scale model was proposed by the meteorologist Smagorinsky (1963) and the model was later developed by many scholars. SGS stress has the following form

$$\tau_{ij} - \frac{1}{3} \tau_{kk} \delta_{ij} = -2\mu_t \bar{S}_{ij} \tag{4}$$

where  $\mu_t$  is the turbulent viscosity of sub-grid scale. In the literature (Felten *et al.* 2004), it is recommended to calculate the turbulent viscosity as follows

$$\mu_t = (C_s \Delta)^2 |\bar{S}| \tag{5}$$

where

$$\bar{S}_{ij} = \frac{1}{2} \left( \frac{\partial \bar{u}_i}{\partial x_j} + \frac{\partial \bar{u}_j}{\partial x_i} \right), |\bar{S}| = \sqrt{2\bar{S}_{ij}\bar{S}_{ij}}, \Delta = (\Delta_x \Delta_y \Delta_z)^{1/3} \tag{6}$$

where  $\Delta_i$  and  $C_s$  represent the grid size along the  $i$ -axis and the Smagorinsky constant, respectively. Theoretically speaking, the Smagorinsky constant is related to the Kolmogorov constant. However,  $C_s$  has to be in practice adjusted at a value lower than the theoretical value in order to minimize the diffusion effects of the sub-grid tensor. Different optimized values of  $C_s$  should be proposed according to the property of the flow field. Its commonly-applied value ranges from 0.1 to 0.15. Tsubokura *et al.* (2010) pointed out that calculated results of a road vehicle's unsteady aerodynamic force in crosswinds is more consistent with the test ones when  $C_s$  is assigned to be 0.10.

### 2.3 Approximate wall boundary condition in large-eddy simulation

For a flow around a bluff body, the turbulence in a boundary layer is an important problem. A large number of tests show that a turbulent flow over a solid wall can be divided into near-wall region (inner region) and core region (outer region) along wall-normal direction. In core region, the turbulence is fully developed while it is not sufficiently developed in the near-wall region. There exists the phenomenon of boundary layer's transition in near-wall region and the laminar flow becomes turbulence there. Near-wall region consists of viscous layer, transition layer and logarithmic-law layer. The viscosity (molecular) and the turbulence play different roles in these sub-layers. There are two kinds of ways to solve near-wall flows: one is multi-zone calculation while the other is to use approximate wall boundary conditions. Multi-zone method uses very fine grids to resolve near-wall region of high Reynolds numbers. Even though great progress has been made in computer technology and computational fluid dynamics in the last several decades, the near-wall resolution is still a problem confronted by us today. It is desirable to use an approximate boundary model in LES simulation for a flow of high Reynolds number over a bluff body. An approximate wall model establishes the relation of physical quantities in near-wall zone with those in core zone by using a set of semi-empirical formulas, which is called the wall functions. Two dimensionless parameters  $u^+$  and  $y^+$ , which denote tangential flow velocity and distance respectively, are used in near-wall functions

$$u^+ = \frac{u}{u_\tau}, y^+ = \frac{\Delta y}{\nu} \sqrt{\frac{\tau_w}{\rho}} \tag{7}$$

where  $u$  is mean tangential velocity,  $\Delta y$  denote the distance from the wall,  $\tau_w$  is wall shear stress,  $u_\tau$

is wall friction velocity and it is equal to  $(\tau_w/\rho)^{1/2}$ . According to the literature (Cabot 1995), when  $y^+ < 5$ , the corresponding region is located in the viscous sub-layer where the tangential velocity presents linear distribution along the wall-normal direction; when  $30 < y^+ < 500$ , the flow is located in a logarithmic-law sub-layer where the tangential velocity presents logarithmic-law distribution. The effect of molecular viscosity and turbulence are equally important in transition layer and it is difficult to use a formula to describe the sub-layer. However, the transition layer is very thin and is usually emerged into logarithmic-law layer in practice.

Xie and Castro (2006) adopted LES-RANS to investigate turbulent flow over arrays of wall-mounted obstacles, in which the wall function was used and  $y^+ = 11.2$  is recommended as the cut-off between viscous sub-layer and logarithmic-law layer. The literature suggested that the flows are not crucially dependent on the near wall regions but dominated by the dynamics of the body-scale motions. Kanda *et al.* (2004) also took the local profile of the tangential velocity component to be logarithmic at all solid surfaces, and obtained reasonable results. The problem investigated by the paper is a flow around a bluff body and the mobile wall boundaries are used. The near-wall grids in the computational domain should be updated repeatedly, which further limits the application of LES-RANS method and the calculation of high resolution in near-wall region. Therefore, the logarithmic profile of the tangential velocity is applied to all wall boundaries in this paper.

#### 2.4 Dynamic mesh method

For the problem in this study, the dynamic mesh technique is adopted to simulate the movement of a vehicle in the computational domain owing to the existence of mobile wall boundaries. In dynamic mesh method, the grids are updated or re-divided according to the new locations of moving wall boundaries in each time step. There are three ways to update grids in computational domain: spring-based smoothing, dynamic layering and local re-meshing method. Spring-based smoothing method does not change the grid topology and need no interpolation. However, when it is used to the cases of large-amplitude movement of wall boundaries, it will lead to the degradation of the grid quality. Dynamic layering method bears the advantage of being fast, but it requires that the grid types in the vicinity of the moving border are hexahedral or wedge-shaped. The requirement is not appropriate for the flow of complex shape. Local re-meshing method is adaptive to triangular (2d) or tetrahedral (3d) grids, and thus it could be used for the flows of complex shape. In this paper, the hybrid method of spring-based smoothing and local re-meshing is used.

The parameters involved in spring-based smoothing method include spring constant factor, boundary node relaxation, convergence tolerance and number of iterations. In this paper, these parameters are set to be 1.0, 1.0, 0.001 and 20, respectively. Local re-meshing method need to set the following parameters: the maximum cell skewness, maximum length scale and the minimum length scale. These parameters are used to determine which grids need to be re-meshed. The maximum cell skewness is assigned at 0.9; the minimum length scale is set as the initial grid size in the encryption region of driving path; and the maximum length scale is set as the maximum grid size of initial grids in the total computation domain. These parameters guarantee that the quality of updated grids is as good as the initial ones. In order to avoid the existence of negative volume during the process of updating grids, the time step should be less than the minimum grid size divided by the traveling velocity.

Since the User-Defined Function (UDF) in Fluent solver can define vehicle models' movement, the paper compiles UDF in C language and defines macros to visit and control Fluent solver. In

this way, one could simulate a vehicle moving in the computational domain.

### 2.5 Numerical solution method

In Fluent solver, the finite volume method (FVM) is adopted to discrete partial differential equations of fluid, which derives discrete equation set from the integral form of fluid's conservation equations. The discrete equation set has concise form and is more easily to be programmed. In FVM, one of the important steps is to derive the physical quantity and its derivative on the interfaces of the control volumes by the interpolation of node quantities, which is called discrete format. Commonly-used discrete formats include central difference format, the first-order upwind format, second-order upwind format, QUICK format, etc. This paper mainly uses second-order upwind format for convection item. Second-order upwind format determines the physical quantities on the interface through the two nodes upstream. The method considers the influence of the curvature of the physical quantity distribution and its cut-off error bears the second-order accuracy. With regard to the diffusion term, the central difference format is adopted. For the steady analysis of fluid, the movement equations consist of convection, diffusion and the source term. And for the transient fluid dynamics problem, the transient item related to the time must be considered. In Fluent solver, the first-order implicit formulation is adopted in the paper since the second-order implicit formulation of transient item is not compatible with the problem of mobile wall boundaries. The solving strategies of discrete equation set could be divided into segregated method and coupled method. Coupled method is to solve the discrete equation sets simultaneously and to obtain the solutions of various physical quantities. Segregated method does not directly solve the equations simultaneously, but solve the algebraic equations sequentially and repeatedly until the convergence of solution is accomplished. In this study, the most widely-used SIMPLE algorithm in the segregated method, namely semi-implicit method for pressure-linked equations, is used in numerical solution.

### 3. Verification of the CFD model

The aerodynamic problems of a vehicle passing through a bridge tower's wake zone involve not only transient aerodynamic phenomena, but also the bluff body aerodynamic interference of the bridge tower, which will be studied by using the computational fluid in this paper. Here, the aerodynamic forces of a simplified vehicle model are calculated and compared with the testing results in the literature (Charuvisit *et al.* 2004a) in order to verify the reasonability of the computational methods and schemes used in the paper. The literature (Charuvisit *et al.* 2004a) studied the aerodynamic force characteristics of moving vehicle models in the wake region of a bridge tower using wind tunnel tests, in which a simplified car model is a cuboid of 160 mm×64 mm×56 mm while the bridge tower model is a cuboid of 144 mm×120 mm×1300 mm. The vehicle's model is 100 mm high from the ground.

As we know, the blunt body inevitably causes the variation of the flow velocity and wind pressure around it, while at the boundaries the wind speed and air pressure are fixed. Thus, the computational domain should be large enough to guarantee the applicability of the boundary conditions, and eliminate the dependence of the results on the size of the computational domain. Compared with the vehicle, a bridge tower is enough high to ignore the effect on the aerodynamic force of the vehicle due to the air flow incised from the top of the bridge tower. However, the width is the main factor among the computational domain's sizes that have the influence on the

calculated results. Here, the vehicle model is laid out within the bridge tower's wake region, and the transverse space between the bridge tower and the vehicle is set as the characteristic length  $B$ . The influence of the computational domain's size on results is studied by using different computational domain schemes. It is noticeable that the length  $B$  includes not only the space between the bridge tower and the vehicle, but also the widths of themselves.

In this paper, unstructured grids are adopted to mesh the computational domain. The grids around the vehicle model, the bridge tower and along the moving path of the vehicle are refined. The detailed grid scheme is set as follows: the vehicle and the bridge tower's surface grids are set to be 15 mm and 30 mm, respectively; the volume cell size along the vehicle's moving path is 15 mm; the volume cell sizes in other regions are 30-200 mm and the growth ratio of grids is set to be 1.30. The boundary conditions are as follows: the entrance boundary is velocity-inlet; the exit is pressure outlet; the side and top boundaries are symmetry boundaries; the bridge tower, the vehicle model and the ground are wall boundaries. LES method is applied to the transient analysis and the residual error is set to be  $1e-4$ . The distribution of the  $y+$  values in the vicinity over the bridge tower and vehicle models is shown as Fig. 1. The figure presents that the  $y+$  values are mainly distributed within the range of 130-350 and they are possibly larger than 400 only in the individual positions of the bridge tower's edges and corners. So it could be said that the first grids near wall boundaries have been laid out in logarithmic-law sub-layer.

The definitions of pneumatic coefficients are available in the literature (Ma *et al.* 2013). Aerodynamic forces are divided by  $1/2\rho(U^2 + V^2)A_f$  to obtain dimensionless coefficients. The symbol  $\rho$  denotes the air density,  $U$  the wind velocity,  $V$  the vehicle's moving velocity, and  $A_f$  the projection area of the van model in the lateral direction. The aerodynamic yawing moments are divided by  $1/2\rho(U^2 + V^2)A_f L$  to obtain the corresponding coefficients. The symbol  $L$  is the distance between the front axis and rear axis of the van. Table 1 gives the different computational domain schemes and the vehicle's lateral aerodynamic force values obtained from the steady CFD. The results show that when the clear width at the entrance is 6 times characteristic length  $B$  and the width at the exit is 3 times characteristic length  $B$ , the dependence of the calculation results on the computation domain's size is eliminated.

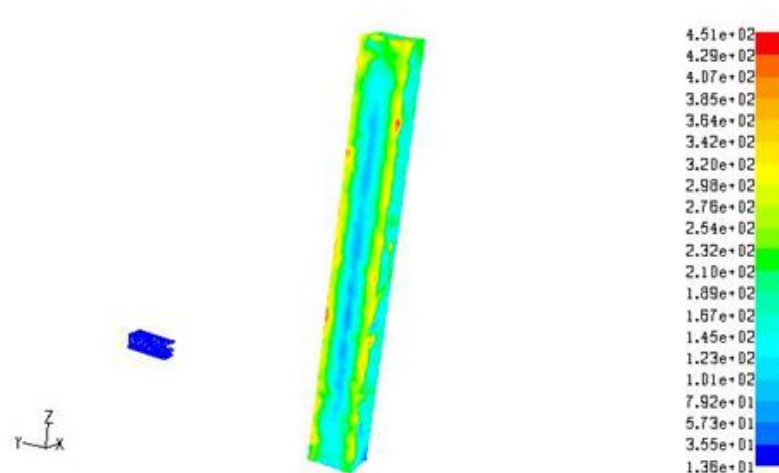
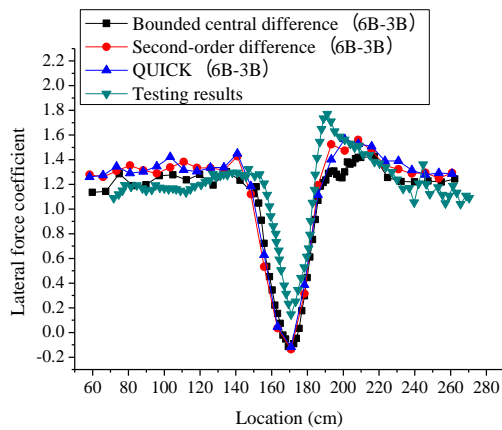


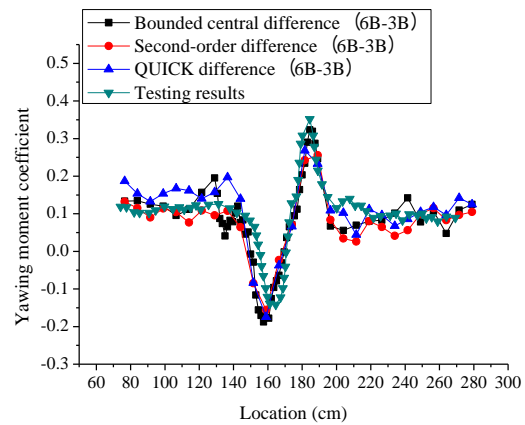
Fig. 1 Distribution of  $y+$  value in the vicinity of the simplified car and tower models

Table 1 Calculated aerodynamic force of a car model in wake zone using different schemes

Serial number	Clear width at the entrance	Clear width at the exit	Grid quantity (million)	Number of iterations	Lateral force (N)
1	1B	1B	0.225	148	0.98
2	3B	1B	0.355	172	0.79
3	6B	1B	0.542	189	0.719
4	9B	1B	0.745	231	0.704
5	1B	3B	0.354	173	0.96
6	1B	6B	0.542	190	0.97
7	6B	3B	0.667	198	0.716



(a) Lateral force coefficients



(b) Yawing moment coefficients

Fig. 2 Aerodynamic coefficients of the simplified car model across the tower using large eddy model

The above-mentioned computational domain is used to calculate the transient aerodynamic force of a moving vehicle when it passes through the bridge tower's wake region. The vehicle runs from 1700 mm left of the tower model to the symmetric position on its right. The wind velocity and traveling velocity are set as the same with that from the literature (Charuvit *et al.* 2004a). The wind velocity is assigned at 10m/s at the entrance of the computational domain. The movement of the vehicle with the speed of 3m/s is implemented using dynamic mesh technology. The calculated aerodynamic force coefficients of the static vehicle and the moving vehicle are given in Figs. 2(a) and 2(b). Figs. 2(a) and 2(b) show that the results of a moving vehicle using

computational fluid analysis agree well with the testing results. The pressure difference between the windward and leeward contributes the majority of the vehicle's lateral aerodynamic force in crosswind. Hence, the method of approximate near-wall function is accurate enough to predict the similar aerodynamic problem in this study.

#### 4. The mechanism of a moving vehicle's unsteady aerodynamic force in crosswind

##### 4.1 Vehicle and bridge model

In this paper, a van, which is one of high-sided vehicles and vulnerable to traffic accidents in a windy environment, is taken as the analysis object to study the aerodynamic forces of a vehicle on a bridge deck or on the flat ground. Detailed settings of the vehicle (e.g., small gaps, sharp corners, etc.) could severely decrease the quality of the generated grids, cause large grid distortion rate, and affect the numerical convergence and accuracy. In order to obtain grids of high quality, the factors which have small impact on the vehicle aerodynamic performance and yet significant influence on grid quality are ignored. These ignored factors include concave and convex objects on vehicle surface (e.g., rear view mirror, door handles, etc.), the small uneven objects at the vehicle bottom. The wheels are cylindrical objects and close to the ground, which forms a sharp angle to the ground. Given that the sharp angle will cause a too large grid distortion rate, the wheels are ignored in the vehicle model in this paper.

At present, no matter in a wind tunnel test or in computational fluid analysis, it is almost impossible to adopt full scale models both for a bridge or vehicles owing to the limitation by the wind tunnel's size or a computer's capacity. Charuvisit *et al.* (2004a), Tsubokura *et al.* (2010) and Cheng *et al.* (2011) investigated the aerodynamic force on a passing vehicle by using the scaled vehicle model of 1:30 or 1:20. In this paper, the 1/20 scale models are used and the outline dimension of the 1/20 scale model of the van is given in Fig. 3. When a wind tunnel test is used to study on the aerodynamic force subjected by a moving vehicle model in crosswind, it is necessary to guide a model to move along the direction of the wind tunnel's width. This is not easy because it implies a high request for the width of a wind tunnel. Owing to the limitation of the tunnel's width, the ratio of traveling velocity to crosswind velocity ( $V/U$ ) are assigned at 0.3, 0.6 and 0.86 for the experiment in the literature (Charuvisit *et al.* 2004a), and the vehicle's traveling velocity was set to be 3m/s in all these cases. In fact, the ratio of  $V/U$  exerts an important influence on the regularities of the aerodynamic force and aerodynamic interference subjected to moving vehicles in crosswind. It should be said that these ratios of  $V/U$  tend to be small. In this study, the velocities of the vehicle and the wind are assigned to be 20m/s and 10m/s, respectively. Thus, the  $V/U$  velocity ratio is 2:1, which is within its normal range and also highlights the influence of vehicles' movement on their lateral aerodynamic forces.

The models of the main beam and the bridge tower involved in the subsequent contents are with the Sutong Yangtze Bridge as example. The bridge has a span of 1,088 meters and had been the longest cable-stayed bridge in the world until 2012. The bridge's towers are inverted Y-shaped reinforced concrete structure and its bridge deck is a steel box girder with fairing noses on both sides. The total width of the bridge deck is 41 m including the fairing noses. Six standard highway lanes in two directions are designed. The 1/20 scale model of the bridge's main girder is shown in Fig. 4, in which the model's length is 5000 mm. Li *et al.* (2009) pointed out that when the Reynolds number is more than  $3E10^5$ , the dependence of the testing or calculating results on the

Reynolds number decrease and the results could be applied to investigate the actual engineering problem. Here, the bridge width of the scale model is 2050 mm, the kinematic viscosity of the air is  $14.8 \times 10^{-6} \text{ m}^2/\text{s}$  and the corresponding Reynolds number is  $1.38 \times 10^6$ , which indicates that the model scale and the Reynolds number are large enough in this study.

#### 4.2 Boundary settings and grid meshing scheme

The reasonable geometric models and scale ratios have been discussed in above paragraphs. Here, the influence of the computational domain's size on the calculated results is discussed. For the aerodynamic problem of the vehicle passing through the bridge tower, the lateral space between the bridge tower and the vehicle is the important characteristic length. For a vehicle on the bridge deck but out of the bridge tower wake region, the bridge width becomes characteristic length. As shown in Fig. 5, the dimensions including the clear widths at the entrance and the exit, the clear height over the vehicle and the clearance under the bridge should be set reasonably. Their influence on the calculated results is studied based on adopting several different computational domain schemes as presented in Table 2.

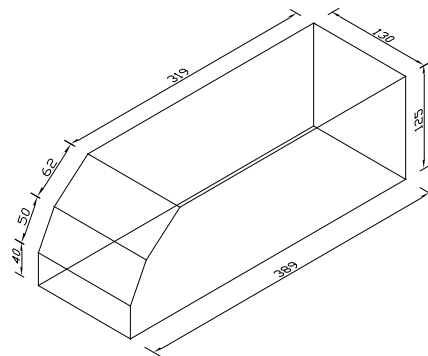


Fig. 3 Geometry model of a van (unit: mm)

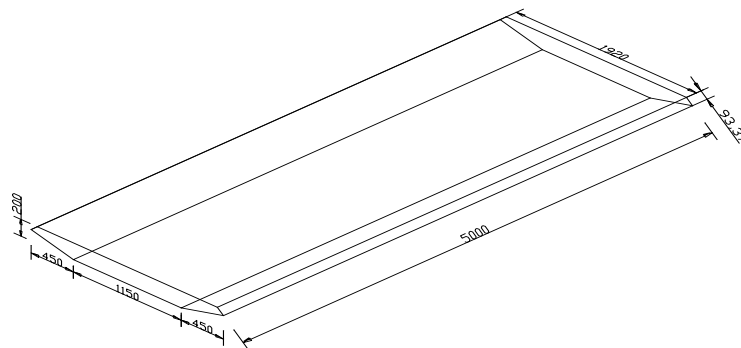


Fig. 4 Geometry model of the bridge' beam (unit: mm)

In all schemes, the computational domain is 7000 mm long. The entrance boundary is set as velocity inlet, the exit is pressure outlet, the side and top boundaries are symmetry boundaries, and the surfaces of the beam and the vehicle model are wall boundaries. The environmental air pressure is the standard atmospheric pressure, the environmental temperature is 300K, the dynamic viscosity of air is  $1.7894 \times 10^{-5} \text{Pa} \cdot \text{s}$  and air density is  $1.225 \text{ kg/m}^3$ . The steady calculation results using those different computational domains are also presented in Table 2. When the clear widths at the entrance and exit are equal to 1.0B, the clear height over the vehicle and the clearance under the bridge are also equal to 1.0B, the dependence of the aerodynamic force on the computational domain's size disappears.

The grid-meshing schemes may also affect the calculated results. Here, the computational domain is divided using unstructured grids. The nodes of unstructured grids are laid out in flow field in an irregular way. This kind of grid bears strong adaptability. In order to ensure the quality of grids, the grid's cell skewness is set to be 0.9 and the growth rate of grids is 1.2~1.3 in the paper. Three kinds of grid meshing schemes are compared as shown in Table 3. The first grid scheme is as follows: surface grids over the vehicle and volume grids along its moving path are set to 15 mm; the surface grids over the bridge's main beam are 30 mm; a size function is applied to the region out of the vehicle's movement path. Other meshing schemes with different maximum grid, and growth rate out of the vehicle's movement path as well as the total grid numbers are provided in Table 3. The steady calculation results using different meshing schemes are also given in Table 3. The lateral aerodynamic force obtained from the above several kinds of meshing scheme bear good consistency, which indicates that the meshing schemes and the number of grids in Table 3 can guarantee the independence of the result on grids. The first kind of grid scheme with the smallest grid numbers will be used in the consequent discussions.

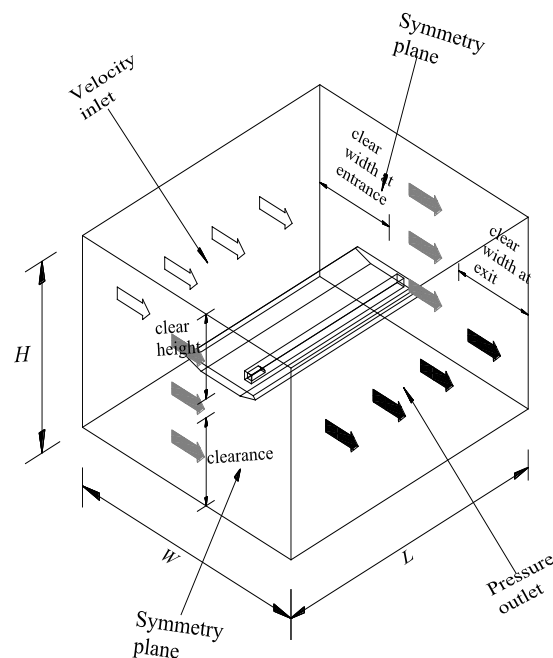


Fig. 5 Computational domain of a van moving on the bridge deck

Table 2 Calculated aerodynamic force of a van model on the deck using different computational domain

Serial number	Clear width at the entrance	Clear width at the exit	Clear height Over the bridge	Clearance under the bridge	Grid quantity (million)	Lateral force (N)
1	0.6B	1B	1B	1B	1.04	3.28
2	0.8B	1B	1B	1B	1.06	3.40
3	1B	1B	1B	1B	1.07	3.47
4	1.2B	1B	1B	1B	1.08	3.47
5	1B	0.6B	1B	1B	1.07	3.45
6	1B	0.8B	1B	1B	1.09	3.50
7	1B	1.2B	1B	1B	1.11	3.47
8	1B	1B	0.6B	1B	1.04	3.43
9	1B	1B	0.8B	1B	1.06	3.41
10	1B	1B	1.2B	1B	1.08	3.47
11	1B	1B	1B	0.6B	1.07	3.46
12	1B	1B	1B	0.8B	1.08	3.46
13	1B	1B	1B	1.2B	1.09	3.47

Note: B is the characteristic length. Here, it denotes the bridge width

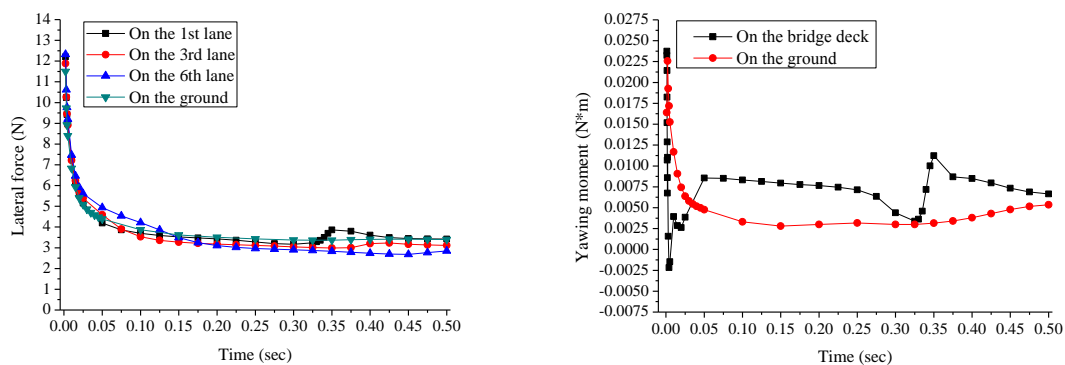
Table 3 Calculated aerodynamic force of a van model on the deck using different grid-meshing schemes

Grid meshing schemes	A	B	C
Surface grid over the vehicle(mm)	15	15	15
Volume grid along the vehicle's movement path (mm)	15	15	15
Surface grid over the main beam(mm)	30	30	30
Minimum grid out of the vehicle's movement path (mm)	30	30	30
Maximum grid out of the vehicle's movement path (mm)	200	180	150
Growth rate of grids out of the vehicle's movement path	1.3	1.25	1.2
Total grid number (million)	1.07	1.20	1.51
Calculated results ( N )	3.47	3.47	3.47

In order to know further about the change of a vehicle's lateral aerodynamic forces, the unsteady analysis is applied to a stationary vehicle. Moreover, the aerodynamic force of the

vehicle on the bridge deck is compared with that of the vehicle model on the flat ground to know about the influence of the main girder's aerodynamic interference on the vehicle. The same computation domain's size and a similar grid scheme are applied to the vehicle on the ground. The ground is set as a wall boundary and its surface grids are set to be 30 mm. The time step in the unsteady analysis is set as 0.001s. Fig. 6 gives the lateral aerodynamic force and yawing moment coefficients of the stationary vehicles on the bridge deck and on the ground. A vehicle's lateral aerodynamic force is much larger than its corresponding value obtained from steady CFD when it just encounters lateral wind. However, it decreases rapidly after a quite short period of time and gradually becomes convergent. Both for the vehicles on the bridge deck and on the ground, their convergent values are the corresponding steady values.

Fig. 7 presents the distributions of pressure coefficient and flow velocity around vehicles on the bridge deck and on the ground at different times. The pressure coefficient is a dimensional physical quantity and it is obtained by dividing relative static pressure by dynamic pressure. Since the lateral wind is blocked on the windward side of the vehicle, the pressure coefficient rises rapidly in the zone and the flow kinetic energy converts to pressure energy there. Then the high wind pressure blocks the lateral wind, making it flow around the vehicle. Consequently, a wind kinetic energy's "transporting channel" comes into being. Fig. 7 shows that at 0.005s, the flow velocity has become quite high in the zones above and below the vehicle, but there still exists a part of air flow acting on the vehicle's windward surface and thus the windward pressure is high. At 0.25s, being blocked by the high wind pressure, the air flow could not approach the vehicle's windward again and its kinetic energy is transported to the leeward side. It could be concluded that after a vehicle encounters a crosswind, the distribution of the pressure coefficient and flow velocity around the vehicle bears a dynamic change process during which its aerodynamic force is also varying with time. With the development of the "transporting channel" of wind kinetic energy, the pressure energy accumulated in the windward zone is alleviated, the wind pressure there decreases and the aerodynamic forces acting on the vehicle become convergent.



(a) Lateral force

(b) Yawing moment

Fig. 6 Unsteady aerodynamic force coefficients of a static vehicle

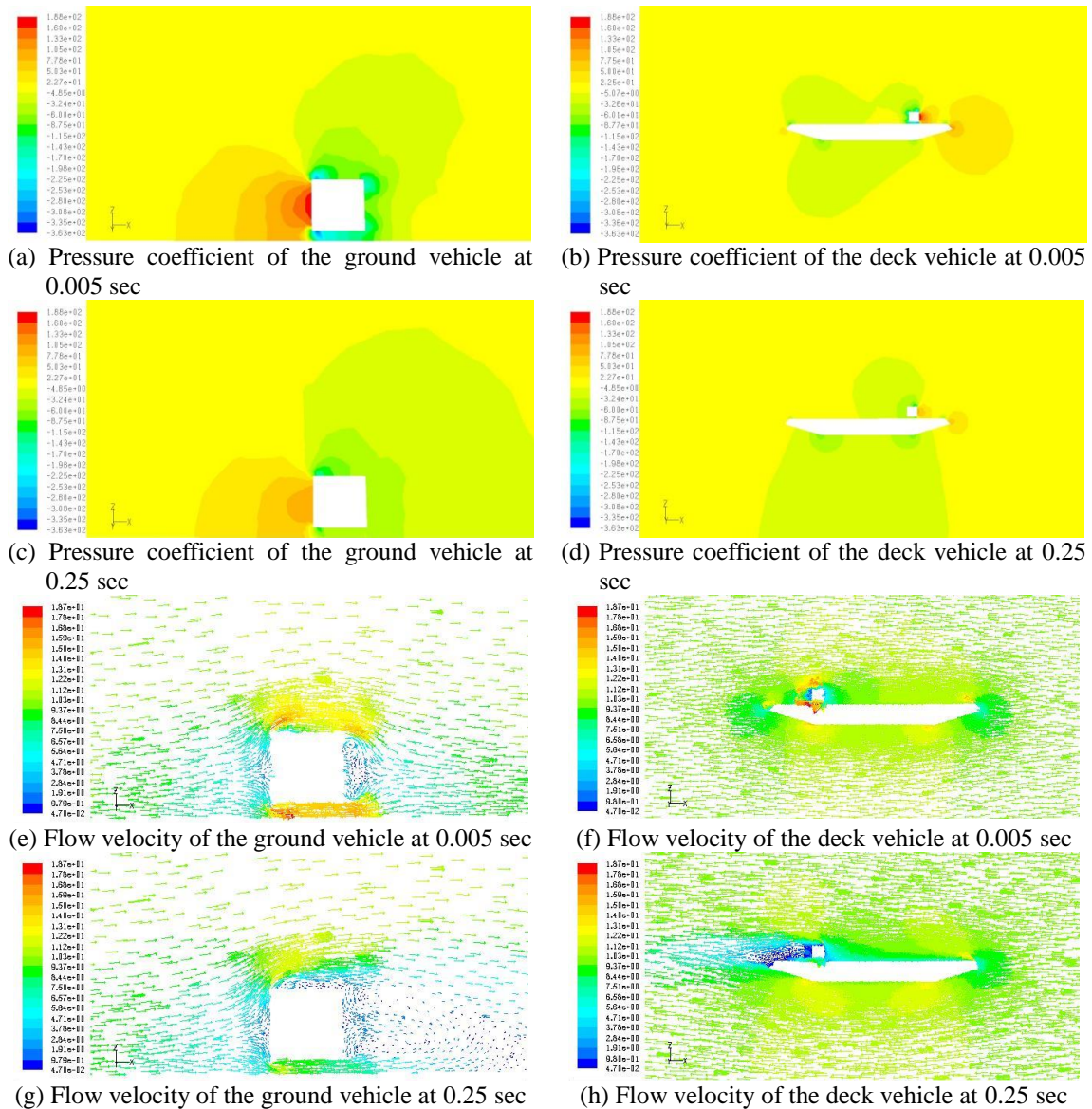


Fig. 7 Pressure coefficient and flow velocity around the static vehicle in crosswind (unit: m/s)

When the vehicle lies on the outermost lane on the windward of the bridge deck (the 1<sup>st</sup> lane), its side force is of no obvious difference from that of the ground vehicle. A little rise occurs to the bridge deck vehicle only at about 0.35s. When the vehicle moves on the innermost lane (the 6<sup>th</sup> lane), its lateral force presents some difference from that of the ground vehicle. The bridge's main beam exerts some influence on the vehicle on the 6<sup>th</sup> lane and makes its convergent rate decreased. The bridge deck vehicle's aerodynamic force is slightly higher than that of the ground vehicle during the period from 0.02s to 0.15s, and yet the former convergence value is smaller than the

latter's. Overall, the influence of the streamlined box girder on the vehicle's lateral aerodynamic force is not very prominent. The more significant aerodynamic interference will come from the bridge tower and other vehicles.

Then, the aerodynamic phenomenon of a moving vehicle in crosswind is analyzed. The vehicle model is laid on the outermost lane on the windward of the bridge deck and the lateral wind is assigned at 10 m/s. The vehicle model's traveling velocity is assigned to be 20 m/s and its movement in computational domain is implemented by using the dynamic mesh method. As previously mentioned, since the analysis of a moving vehicle involves moving boundaries and grid update problems, the smallest grid size should be larger than the product of the vehicle's traveling velocity and the time step in order to avoid the existence of negative volume. Here, both the surface grid over the vehicle model and the volume grid along its movement path are 15 mm, and the traveling velocity is 20 m/s. Thus, the time step length should be less than  $15 \times 10^{-3} / 20 = 7.5 \times 10^{-4}$  s. Given that it is still possible to produce grids less than 15 mm during the process of grid update, this paper sets the minimum length scale to be 15 mm in dynamic meshing parameters, i.e., the grids less than 15 mm need to be updated. Moreover, after several trials, the time step is set to be  $2 \times 10^{-4}$  s. These settings ensure that the grid updating could be smoothly processed.

Fig. 8 gives the aerodynamic force coefficients of moving vehicles on the bridge deck in crosswind. Similar to the situation of a stationary vehicle, the wind pressure at the windward side of a moving vehicle rise rapidly when it just encounters a crosswind, and it decreases rapidly, and then becomes "convergent" after a short period. However, the "convergent" values are much greater than a stationary vehicle's corresponding values. As we know, the vehicle's forward movement could not cause the lateral force and yawing moment directly. Then, what causes the larger lateral force on a mobile vehicle? Combined with Fig.6, one could deduce as follows: after a short period of time, the lateral aerodynamic force of a vehicle's rear part has been decreased to some extent due to the development of the wind kinetic energy's "transportation channel", while its front part suffers more lateral pressure difference because of its arrival at a new region. So the "transportation channel" of the wind kinetic energy around a moving vehicle could not reach a steady state that occurs to a stationary vehicle. Although a mobile vehicle's aerodynamic force also presents a "convergent" trend, it is because the following two factors: one is the wind kinetic energy's "transportation channel" which causes the decrease of the aerodynamic force at the vehicle rear part; the other one is that the vehicle front part suffers more force because of its arrival at a new region. Those two factors offset each other, so the "convergent" value of a moving vehicle's lateral force is much larger than that of a stationary vehicle. It could be further deduced that the faster the vehicle moves, the larger its lateral force's "convergent" value will be. If the moving velocity of the vehicle was not a constant, the "balanced state" would be broken and a large fluctuation would occur to the vehicle's lateral force. The front and rear parts of a mobile vehicle bear different wind pressure difference, which makes a moving vehicle bear much more yawing moment than a stationary one.

Fig. 8 also compares the results using different time steps and different residual errors. It is necessary to choose the double-precision CFD solver when the residual error is set to be  $1.0 \times 10^{-5}$ . Compared with a stationary vehicle whose lateral force curve with time is smooth, the results for the moving vehicle involve many small fluctuations. These small data fluctuations cannot be removed by using the residual error of  $1.0 \times 10^{-5}$ , which indicates that these fluctuations are not caused by the numerical truncation error in computer. The interpolation of physical quantities during the process of updating grids may be the main cause of the fluctuation. In spite of this, the calculation results using the time step of  $1 \times 10^{-4}$  match well with the results from using the time step

of  $2e-4$ , which suggests that these errors only cause the local fluctuation of data instead of accumulating and changing the trend of the aerodynamic force. In view of these characteristics of a moving vehicle's lateral aerodynamic phenomenon, no matter in computational fluid analysis or in the wind tunnel test, the information is insufficient if only using a stationary vehicle model.

### 5. The regularity and mechanism of the vehicle passing through a bridge tower's wake region

Taking the Sutong Yangtze Bridge as the example, this section discusses the characteristics of the van's aerodynamic force coefficients when it moves on the bridge deck and goes through the bridge's tower. The 1:20 scale geometric sizes of the bridge tower are given in Fig. 9. Apparently, only a part of the bridge tower, which is adjacent to the bridge deck, exerts the aerodynamic interference on the vehicle. The segmental model of the bridge tower is 2000 mm high, which is 16 times as much as the vehicle model's height. The width of the computational domain, which is used for the calculation of the aerodynamic force of the vehicle passing through a bridge tower, is associated with not only the transverse interval between the vehicle and the tower model, but also the bridge's width. Here, the transverse interval and the bridge width are regarded as two characteristic lengths  $B_1$  and  $B_2$ , which are equal to 853 mm and 2050 mm respectively. According to the aforementioned analyses, the clear width is set to  $\text{Max}\{3B_1, B_2\}=2559$  mm at the entrance of the computational domain while the clear width is set as  $\text{Max}\{B_1, B_2\}=2050$  mm at the exit; both the clear height over the bridge deck and the clearance under the bridge deck are set to 2050 mm. The total width of the computational domain is 6659 mm, and its length and height are 7000 mm and 4450 mm, respectively. Fig. 10 gives the computational domain of a van passing through the bridge tower.

The boundary conditions of the computational domain are identical with the case of the vehicle moving on the bridge deck. The crosswind and traveling velocity are assigned to be 10 m/s and 20 m/s, respectively.

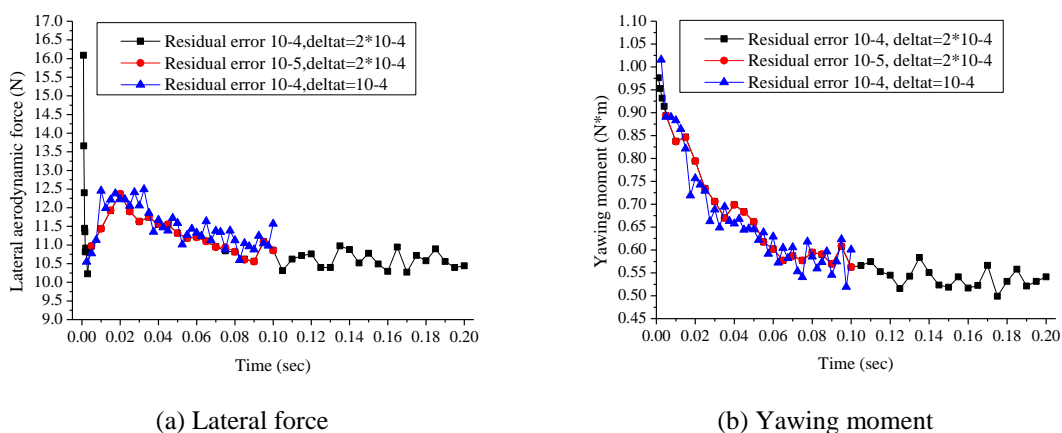


Fig. 8 Unsteady aerodynamic force of a moving vehicle on the deck in crosswind

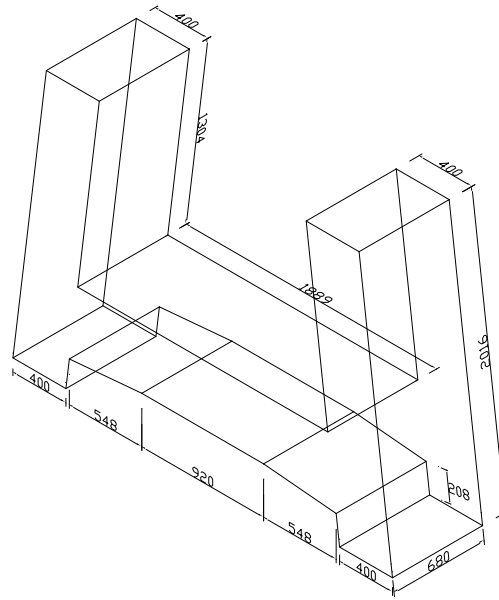


Fig. 9 Geometry model of the bridge tower (unit : mm)

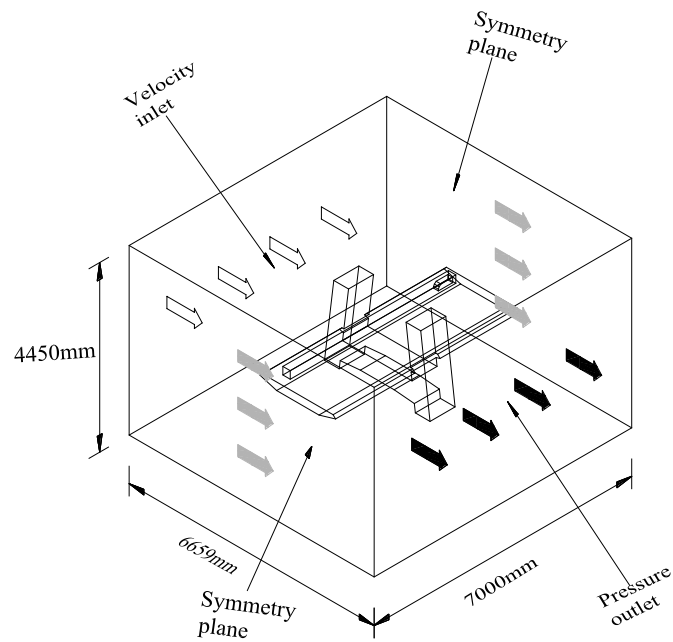


Fig. 10 Computational domain of a van passing through the bridge tower

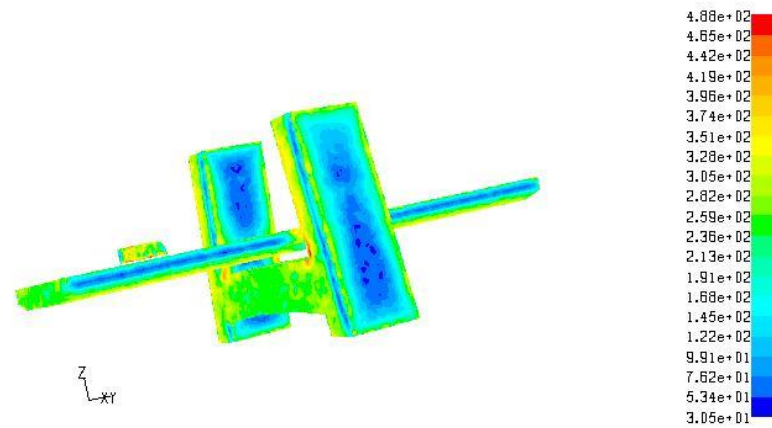


Fig. 11 Distribution of  $y^+$  value around the wall boundaries

Unstructured grids are applied to mesh the computational domain and the detailed grid scheme is as follows: the surface grids on the vehicle are 15mm, and the surface grids on the main girder and the bridge tower are 30 mm; the volume grids along the vehicle's movement path are 15 mm; the minimum and maximum volume grid of the rest zones are 30 mm and 300 mm, respectively, and the grid growth rate is 1.3. The total grid number is 1.45 million. The calculating time step length is set to be 0.0002s and 1000 time steps are analyzed. Large eddy simulation method is used to analyze this case. The movement of the vehicle model is implemented by using dynamic grid method and the uniform wind velocity is applied to the velocity-inlet of the computational domain. Fig. 11 presents the distribution of  $y^+$  value of a van going through the Sutong Yangtze Bridge's tower. The result indicates that the first grids in the vicinity of the wall boundaries are distributed in logarithmic-law layer.

Fig. 12 gives the aerodynamic force coefficients of the van when it goes through the bridge tower at a high speed. Lateral force and yawing moment coefficients of the vehicle are the largest at the starting time. The reason is that the air flow is blocked on the vehicle's windward side, and then the high wind pressure rapidly accumulates there when the vehicle just encounters the action of the lateral wind. The aerodynamic force mechanism of a moving vehicle, to which enough attention is paid in aforementioned content, plays a role here. After the vehicle passes through the bridge tower's wake zone, its aerodynamic forces are consistent with those of the above-mentioned single vehicle moving on the bridge deck without the interference of the tower. The lateral force and yawing moment coefficients decrease suddenly when the vehicle enters into the wake region and reach their minima on the leeward side of the bridge tower. When the vehicle goes through the bridge tower's wake zone on the outermost lane on the windward of the bridge deck, its aerodynamic force coefficients becomes quite large negative values. When the vehicle gets out of the wake region, its side aerodynamic force and moment are evidently more than the value when it just enters into the wake region. Experimental results in the literature (Charuvisit *et al.* 2004a) also support the viewpoint of the asymmetric distribution of the vehicle's aerodynamic force on two sides of the bridge tower.

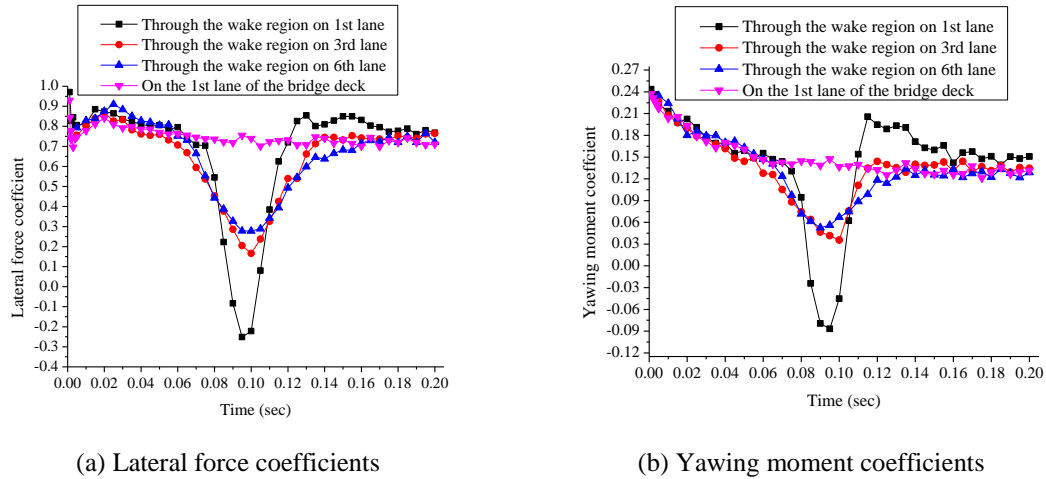


Fig. 12 Aerodynamic coefficients of a van going through the Sutong Bridge's tower

When the vehicle passes through the wake zone on the innermost lane on the windward (the 3<sup>rd</sup> lane) or on the outermost lane on the leeward (the 6<sup>th</sup> lane) of the bridge deck, its side aerodynamic force and yawing moment also reaches their valley values on the leeward of the bridge tower. However, these values are much larger than those of the vehicle through the tower on the 1<sup>st</sup> lane. And in these cases, no negative values occur in the side aerodynamic force and moment. When the vehicle leaves the bridge tower's leeward side on one of these two lanes, its aerodynamic force and moment do not rise but become convergent with that of the vehicle not through the bridge tower.

Figs. 13(a)-13(d) give the flow velocity and pressure coefficient distribution in the wake region of the bridge tower. Combining with the distribution of the flow velocity and pressure coefficient, the reason can be explored for the aerodynamic regularity of the vehicle passing through the bridge tower. Fig. 13(a) shows that there appear two symmetrical vortices and a backflow region forms on the bridge tower's leeward. And the vehicle moving on outermost lane on the windward just passes through this region, so both its side force and yawing moment coefficients will become negative as soon as it arrives at the leeward side of the bridge tower. Fig. 13(b) shows that when the vehicle crosses the wake region, the backflow structure there was broken into pieces. Therefore, when it gets out of the wake region, the high-velocity flow will have impact on the windward of the vehicle directly while it could not enter into the backflow region and change its direction again. So the wind pressure on the vehicle's windward is obviously higher when the vehicle exited the wake zone than that when the vehicle entered the wake region, which could be observed clearly in Figs. 13(c) and 13(d). When the vehicle passes through the wake zone on the 3<sup>rd</sup> or the 6<sup>th</sup> lanes of the bridge deck, it keeps enough transverse distance from the backflow region, which is the reason that there exist no negative side force and yawing moment coefficients. However, the whole leeward region of the bridge tower belongs to low-velocity region, and the aerodynamic forces of the vehicles on the 3<sup>rd</sup> or the 6<sup>th</sup> lane still reach their valley values there. And in these cases, the vehicle would not ruin the structure of the backflow in the wake region of the tower. So its side force and moment would not rise when it gets out of the wake region.

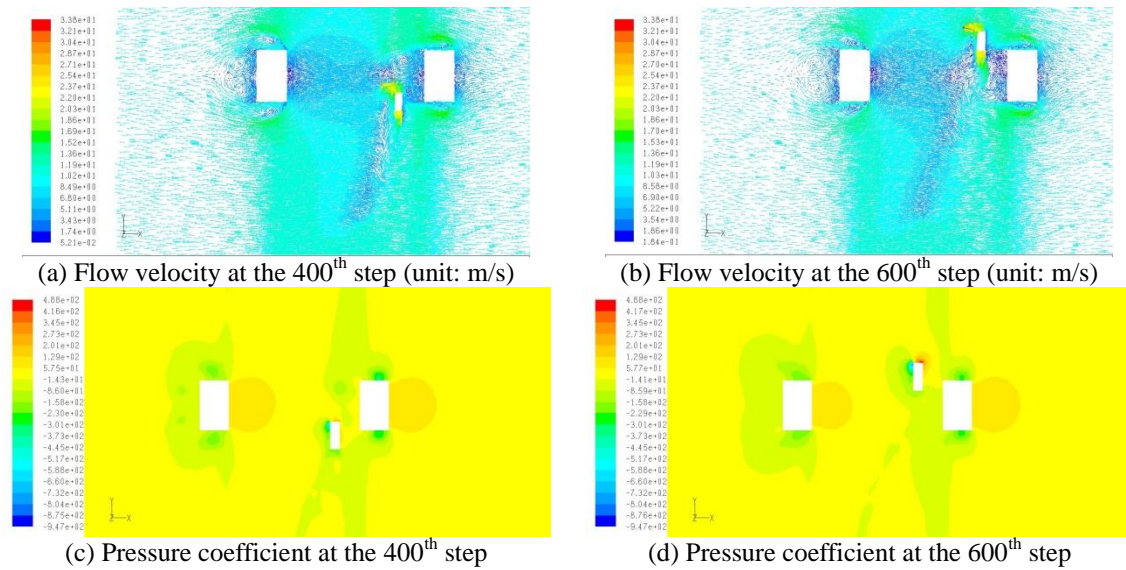


Fig. 13 Flow velocity and pressure coefficient in the bridge tower's wake zone

## 6. Conclusions

Based on large eddy simulation together with dynamic grid technique, the paper uses CFD to study the transient aerodynamic force mechanism of the vehicle in crosswind and the regularity of dynamic aerodynamic interference on the bridge deck. By comparing the CFD results with the wind tunnel test results from the corresponding literature, the method adopted in the paper of modeling a vehicle in the wake region of a bridge tower is verified. Through observing the aerodynamic force of a moving vehicle on Sutong Bridge, the mechanism and regularities for such case were explored in this study. The conclusions drawn from the study are as follows:

1) The width of the computational domain has important influence on the calculation results. For a vehicle moving on a bridge deck and without other aerodynamic interference, the bridge deck's width could be the characteristic length  $B$ . When the clear widths at the entrance and the exit of the computational domain, the clear height over the bridge model and the clearance under it are all as large as the deck's width, the calculation results will be independent on the size of the computational domain. For a vehicle passing through a bridge tower's wake zone, the transverse interval between the vehicle and the tower should be the characteristic length. When the clear widths at the entrance and exit are up to 6 times and 3 times characteristic length respectively, the calculation result is not dependant on the computational domain's width again.

2) A vehicle's lateral aerodynamic force is much larger than that from the corresponding steady analysis when the vehicle just encounters the crosswind. The lateral aerodynamic force decreases rapidly and converges to the steady analysis value after a short period of time. This is because the crosswind is blocked on the vehicle's windward side, the high wind pressure accumulates on its windward instantly, and the wind kinetic energy is converted into wind pressure potential energy there. But since the high pressure in turn hinders the crosswind's impact on the windward of the vehicle, the air flow is forced into flowing up and down the vehicle, and the wind kinetic energy is transported into its leeward. After the "transporting channel" of the wind kinetic energy around the

vehicle is developed, the pressure energy accumulated on the windward is alleviated, and the pressure difference between the windward and the leeward decreases. Then, the aerodynamic force of the vehicle tends to be convergent.

3) A moving vehicle's lateral force also presents a convergent trend when it moves at a constant speed. But the "convergence" is resulted from a decrease of wind pressure over the vehicle's rear part and the increase of the vehicle's front part. The two factors offset each other and make the vehicle keep a balanced state. The convergence value of a mobile vehicle's lateral force is much greater than that of a stationary vehicle. Furthermore, the difference of the development degree between the flow around a moving vehicle's front part and that around its rear part makes the vehicle's yawing moment be larger than that of a stationary one. So, a mobile vehicle's aerodynamic force in crosswind is a complex transient aerodynamic problem, which cannot be concluded by using the results from a steady calculation or test.

4) A vehicle's aerodynamic force coefficient decreases suddenly when it enters into the wake region and reaches its minimum value on the leeward of the bridge tower. There exists a backflow region on a bridge tower's leeward. When the vehicle moves on the outermost lane on the windward of the bridge deck and just passes through the backflow region, it will encounter negative lateral aerodynamic force and yaw moment in the bridge tower's wake zone. And the vehicle's passing ruins the original vortex structure of the backflow region. That will lead to the result that the lateral wind on the right side of the bridge tower, which is originally involved in the backflow, does not change its direction but directly impact on the windward side of the vehicle. So when the vehicle leaves from the backflow region, it will suffer stronger aerodynamic force than that when it just enters into the region. If the vehicle crosses the bridge tower on the innermost lane on the windward, or on the outermost lane on the leeward of the bridge deck, the vehicle and the backflow structure on the bridge tower's leeward do not mutually influence each other. In this case, the vehicle's pneumatic safety performance is evidently better than that of the vehicle on the outermost lane on the bridge deck's windward.

An overtaking or meeting process in a strong crosswind environment also exerts non-ignorant influence on the pneumatic safety of a vehicle moving on a large bridge with high elevation, which will be paid a special attention to in further research. In addition, given that the small cross-section size of a bridge's railings brings much difficulty in the unsteady fluid analysis, its influence on vehicles' lateral aerodynamic forces is not included in this study, but should be investigated in further studies.

## Acknowledgements

The authors acknowledge the financial contributions by Grant of China national natural science foundation (51108154, 51278064).

## References

- Bettle, J., Holloway, A.G.L. and Venart, J.E.S. (2003), "A computational study of the aerodynamic forces acting on a tractor-trailer vehicle on a bridge in cross-wind", *J. Wind Eng. Ind. Aerod.*, **91**(5), 573-592.
- Breuer, M., Jaffrézic, B. and Arora, K. (2008), "Hybrid LES-RANS technique based on a one-equation near-wall model", *Theor. Comp. Fluid Dyn.*, **22**(3), 157-187.

- Cabot, W.H. (1995), "Large-eddy simulations with wall models", *Center for Turbulence Annual Briefs*, Stanford Univ., 12, 41-55.
- Cai, C.S., Hu, J.X., Chen, S.R., Zhang, W. and Kong, X. (2015), "A coupled wind-vehicle-bridge system and its applications: a review", *Wind Struct.*, **20**(2), 117-142.
- Cai, C.S., Zhang, W., Liu, X.Z., Peng, W., Chen, S.R., Han, Y. and Hu, J.X. (2013), "Framework of wind-vehicle-bridge interaction analysis and its applications", *J. Earthq. Tsunami*, **7**(3), 132-141.
- Charuvisit, S., Kimura, K. and Fujino, Y. (2004a), "Experimental and semi-analytical studies on the aerodynamic forces acting on a vehicle passing through the wake of a bridge tower in cross wind", *J. Wind Eng. Ind. Aerod.*, **92**(4), 740-780.
- Charuvisit, S., Kimura, K. and Fujino, Y. (2004b), "Effects of wind barrier on a vehicle passing in the wake of a bridge tower in cross wind and its response", *J. Wind Eng. Ind. Aerod.*, **92**(s7-8), 609-639.
- Chen, S.R. and Cai, C.S. (2004), "Accident assessment of vehicles on long-span bridges in windy environment", *J. Wind Eng. Ind. Aerod.*, **92**(12), 991-1024.
- Cheng, S.Y., Tsubokura, M., Nakashima, T., Nouzawa, T. and Okada, Y. (2011), "A numerical analysis of transient flow past road vehicles subjected to pitching oscillation", *J. Wind Eng. Ind. Aerod.*, **99**(99), 511-522.
- Felten, F., Fautrelle, Y., Terrail, Y.D. and Metais, Q. (2004), "Numerical modelling of electromagnetically-driven turbulent flows using LES methods", *Appl. Math. Model.*, **28**(1), 15-27.
- Han, W.S., Ma, L., Cai, C.S., Chen, S.R. and Wu, J. (2015), "Nonlinear dynamic performance of long-span cable-stayed bridge under traffic and wind", *Wind Struct.*, **20**(2), 249-274.
- Han, W.S., Ma, L. and Liu, J.X. (2010a), "Lateral coupling relations between the vehicle-bridge systems under crosswind", *China Civil Eng. J.*, **43**(10), 73-82.
- Han, W.S., Ma, L. and Liu, J.X. (2011), "Research on coupling vibration of wind-vehicle-bridge system with considering driver behavior", *China J. Highway Transport*, **24**(1), 42-49.
- Han, W.S., Ma, L., Yuan, S.J., Chen, A.R. and Liu, J.X. (2010b), "Probability analysis of bridge deck side wind-induced vehicle accidents based on joint distribution of wind speed and wind direction", *China J. Highway Transport*, **23**(2), 43-49.
- Han, Y., Cai, C.S., Zhang, J.R., Chen, S.R. and He, X.H. (2014), "Effects of aerodynamic parameters on the dynamic responses of road vehicles and bridges under cross winds", *J. Wind Eng. Ind. Aerod.*, **134**, 78-95.
- Han, Y., Hu, J.X., Cai, C.S., Chen, Z.Q. and Li, C.G. (2013), "Experimental and numerical studies of aerodynamic forces on vehicles and bridges", *Wind Struct.*, **17**(2), 163-184.
- Han, Y., Liu, S.Q., Cai, C.S., Zhang, J.R., Chen, S.R. and He, X.H. (2015), "The influence of vehicles on the flutter stability of a long-span suspension bridge", *Wind Struct.*, **20**(2), 275-292.
- Kanda, M., Moriwaki, R. and Kasamatsu, F. (2004), "Large-eddy simulation of turbulent organized structures within and above explicitly resolved cube arrays", *Bound. - Lay. Meteorol.*, **112**(2), 343-368.
- Li, J.W., Zhang, H.J. and Han, W.S. (2009), "Wind-induced response of cable-stayed bridge with consideration of Reynolds number effect", *China J. Highway Transport*, **22**(2), 42-47.
- Li, Y.L., Chen, N., Cai, X.T. and Qiang, S.Z. (2010), "Wake effect of bridge tower on coupling vibration of wind-vehicle-bridge system", *China J. Southwest Jiaotong Univ.*, **45**(6), 875-881+887.
- Li, Y.L., Hu, P., Zhang, M.J. and Liao, H.L. (2009), "Wind tunnel test with moving vehicle model for aerodynamic forces of vehicle-bridge systems under cross wind", *Proceedings of the 7th Asia-Pacific Conference on Wind Engineering*, November 8-12.
- Ma, L., Han, W.S., Ji, B.H. and Liu J.X. (2015), "Probability of overturning for vehicles moving on a bridge deck in a wind environment considering stochastic process characteristics of excitations", *J. Perform. Constr. Fac.*, **29**(1), 1-11.
- Rocchi, D., Rosa, L., Sabbioni, E., Sbroisi, M. and Belloli, M. (2012), "A numerical-experimental methodology for simulating the aerodynamic forces acting on a moving vehicle passing through the wake of a bridge tower under cross wind", *J. Wind Eng. Ind. Aerod.*, **104**(3), 256-265.
- Smagorinsky, J. (1963), "General circulation experiments with primitive equations", *Mon. Weather Rev.*, **91**(3), 99-164.
- Snæbjörnsson, J.T., Baker C.J. and Sigbjörnsson, R. (2007), "Probabilistic assessment of road vehicle safety

- in windy environments”, *J. Wind Eng. Ind. Aerod.*, **95**, 1445-1462.
- Tsubokura, M., Nakashima, T., Kitayama, M., Ikawa, Y., Doh, D.H. and Kobayashi, T. (2010), “Large eddy simulation on the unsteady aerodynamic response of a road vehicle in transient crosswinds”, *Int. J. Heat Fluid Fl.*, **31**(6), 1075-1086.
- Wang, B., Xu, Y.L., Zhu, L.D., Cao, S.Y. and Li, Y.L. (2013), “Determination of aerodynamic forces on stationary/moving vehicle-bridge deck system under crosswinds using computational fluid dynamics”, *Eng. Appli. Comput. Fluid Mech.*, **7**(3), 355-368.
- Xie, Z.T. and Castro, I.P. (2006), “LES and RANS for turbulent flow over arrays of wall-mounted obstacles”, *Flow Turbul. Combust.*, **76**, 291-312.
- Xu, Y.L. and Guo, W.H. (2003), “Dynamic analysis of coupled road vehicle and cable-stayed bridge systems under turbulent wind”, *Eng. Struct.*, **25**(4), 473-486.
- Zhu L.D., Li, L., Xu, Y.L. and Zhu Q. (2012), “Wind tunnel investigations of aerodynamic coefficients of road vehicles on bridge deck”, *J. Fluid. Struct.*, **30**, 35-50.

AD